A laboratory study of water ice erosion by low-energy ions

Monthly Notices
of the
ROYAL ASTRONOMICAL SOCIETY

MNRAS **462,** 3361–3367 (2016)
Advance Access publication 2016 July 30

doi:10.1093/mnras/stw1855

A laboratory study of water ice erosion by low-energy ions

Elena A. Muntean,[1★] Pedro Lacerda,[1,2] Thomas A. Field,[3★] Alan Fitzsimmons,[1] Wesley C. Fraser,[1] Adam C. Hunniford[1] and Robert W. McCullough[1,3★]

[1]*Astrophysics Research Centre, School of Mathematics and Physics, Queen's University Belfast, BT7 1NN, UK*
[2]*Max Planck Institute for Solar System Research, Göttingen, D-37191, Germany*
[3]*Centre for Plasma Physics, School of Mathematics and Physics, Queen's University Belfast, BT7 1NN, UK*

Accepted 2016 July 22. Received 2016 July 22; in original form 2015 October 8

ABSTRACT

Water ice covers the surface of various objects in the outer Solar system. Within the heliopause, surface ice is constantly bombarded and sputtered by energetic particles from the solar wind and magnetospheres. We report a laboratory investigation of the sputtering yield of water ice when irradiated at 10 K by 4 keV singly ($^{13}C^+$, N^+, O^+, Ar^+) and doubly charged ions ($^{13}C^{2+}$, N^{2+}, O^{2+}). The experimental values for the sputtering yields are in good agreement with the prediction of a theoretical model. There is no significant difference in the yield for singly and doubly charged ions. Using these yields, we estimate the rate of water ice erosion in the outer Solar system objects due to solar wind sputtering. Temperature-programmed desorption of the ice after irradiation with $^{13}C^+$ and $^{13}C^{2+}$ demonstrated the formation of ^{13}CO and $^{13}CO_2$, with ^{13}CO being the dominant formed species.

Key words: astrochemistry – molecular processes – solid state: volatile – methods: laboratory: molecular.

1 INTRODUCTION

Water ice is a major component of solid bodies in the outer Solar system and played a major role in the planet-formation process (Lunine 2006). Beyond ∼4 au it is not warm enough for water ice to undergo substantial sublimation, resulting in potential lifetimes of order of the age of the Solar system and its observed presence on the surfaces of moons and Kuiper Belt objects e.g. Guilbert et al. (2009), Dalton et al. (2010), Brown, Schaller & Fraser (2012). Water ice, however, will still undergo erosion due to dust and macroscopic body impact and irradiation by cosmic rays, ions in the solar wind (SW) and, for moons and ring particles, magnetospheric ions. Chemical species can be lost from or redistributed on surfaces as a result of this bombardment and new chemical species can be formed (Johnson 1990; Hudson & Moore 2001). Some of the newly formed species will remain embedded in the ice, changing its chemical composition, whilst others may in turn be ejected from the surface. This process has been observed in laboratory ion irradiation experiments involving ices e.g. Brunetto et al. (2006). In some cases, sputtering leads to the formation of thin atmospheres made of water molecules, its dissociation products plus the sputtering species; these have been observed around Jovian and Saturnian satellites (e.g. Hall et al. 1995; Brown & Hill 1996; Johnson et al. 2008). Additionally, energetic ion sputtering is at least partly responsible for global compositional changes across Tethys and Mimas (Schenk et al. 2011).

Sputtering of H_2O ice has been intensively studied in laboratory experiments with both low-energy ions (below 10 keV) and high-energy ions (from 10 keV to a few MeV). Almost four decades ago, Brown et al. (1978) reported pioneering experiments in the sputtering of water ice by H^+, He^+, C^+ and O^+ ions with MeV energies; they reported that the sputtering yield of molecules ejected from water ice per incident MeV ion was higher than predicted by contemporary theory. Brown et al. continued this sputtering work and found that at high energies electronic processes are dominant (Brown et al. 1980). An electronic process represents the interaction of the projectile ions with the electrons of the target and will mostly produce ionization and excitation (Sigmund 1981). Cooper & Tombrello (1984) used 1.6–2.5 MeV ^{19}F ions to sputter water ice and concluded that sputtering yields are sensitive to the charge state of the ion, but independent of ice thickness and temperature below 60 K. Subsequent investigators confirmed no dependence on ice thickness or temperature at $T < 60$ K (Bar-Nun et al. 1985; Baragiola et al. 2003), with the latter study finding no variation up to $T = 140$ K. Furthermore, Johnson et al. (1983) found that water ice has a yield of 10 molecules per ion at 10 K when bombarded with 1.5 MeV He^+, which was in good agreement with the results obtained by Brown et al. (1978). Other experimental studies of high-energy ion sputtering on water ice have reported dependences on temperature and angle of incidence (Teolis et al. 2005; Vidal, Teolis & Baragiola 2005; Teolis, Shi & Baragiola 2009). The formation of

★ E-mail: emuntean01@qub.ac.uk (EAM); t.field@qub.ac.uk (TAF); Rw.McCullough@qub.ac.uk (WMC)

CO_2 from 30 keV energy ion bombardment of H_2O ice was studied by Strazzulla et al. (2003b) and Lv et al. (2012).

The energies and masses that make up the ion-sputtering population depends strongly on environment, whether the icy surface is within a planetary magnetosphere, within the distant SW or exposed solely to the galactic cosmic ray population when outside the solar heliopause (Florinski et al. 2013). The ion-population abundances and energies can be very different between these regions, and hence it is important to measure the sputtering yield (equivalent to the erosion rate) as a function of ion species and energy. This in turn allows modelling of the erosion rate and the amount of liberated material. Bar-Nun et al. (1985) used 0.5–6 keV H^+ and Ne^+ ions to irradiate water ice and observed the sputtered species H_2, O_2 and H_2O. Baragiola et al. (2003) critically analysed data from Bar-Nun et al. (1985) to determine normal incidence sputtering yields due to, for example, 2–6 keV Ne^+ ion impact. Christiansen, Carpini & Tsong (1986) measured the sputtering yields from different ices at 78 K when bombarded with 4 keV Ar^+, Ne^+, N^+ and He^+. Finally, sputtering of water ice at 80 K by 2 keV He^+ and Ar^+ ions at normal incidence was investigated by Famá, Shi & Baragiola (2008), who also considered all the available data from previous experimental studies to propose a formula to predict the sputtering yield from water ice at any temperature by ions of any mass with energies of up to 100 keV.

At heliocentric distances of $R_h \simeq 20$–50 au, the SW plasma has cooled to ∼1 eV so that the ion energy is dominated by the bulk outward flow (Bagenal et al. 1997). With a SW velocity of ∼450 km s^{-1}, the kinetic energy of the ions is therefore $\simeq m_{ion}$ keV, implying that low-energy ion bombardment similar to the above experiments will be important in the Centaur region and the Kuiper Belt. Therefore, to accurately model the interaction between SW and distant atmosphereless surfaces, it is important to test the validity of the Famá et al. (2008) formula for the erosion rate of water ice. In this paper, we present the results of experiments on the sputtering of water ice by 4 keV singly charged ions (C^+, N^+, O^+ and Ar^+) and 4 keV doubly charged ions (C^{2+}, N^{2+} and O^{2+}), and compare them to theoretical predictions and previous experimental data. Additionally, we report temperature-programmed desorption (TDP) measurements of H_2O ice following sputtering by C^+ and C^{2+}. For all carbon ion experiments, we used the isotope ^{13}C, but for clarity, we do not designate this isotope when discussing C-ion processes.

2 EXPERIMENTAL DETAILS

The experimental equipment used in this work was described in detail in Muntean et al. (2015) and will only be briefly presented here. The full apparatus is comprised of two main parts; a low-energy ion accelerator and an ultrahigh vacuum interaction chamber. The ion source is separated from the target chamber by over 4 m of vacuum tubes with four stages of differential pumping. Furthermore, the pressure of source gas in the ion source is typically 10^{-5} mbar. For all these reasons, the level of contamination from the ion source to the target chamber is negligible. Singly and doubly charged ions with energies up to 10 keV are focused and collimated before directed on to the interaction chamber which had a base pressure of 1×10^{-9} mbar. The intensity of the ion beam is measured with a translatable Faraday Cup, which could be positioned in front of the sample. During irradiation, a 90 per cent transmission metal mesh is used to monitor the ion beam current.

Water ice films were deposited on to a KBr substrate at $T = 10$ K and surrounded by a gold-plated radiation shield at $T = 48$ K.

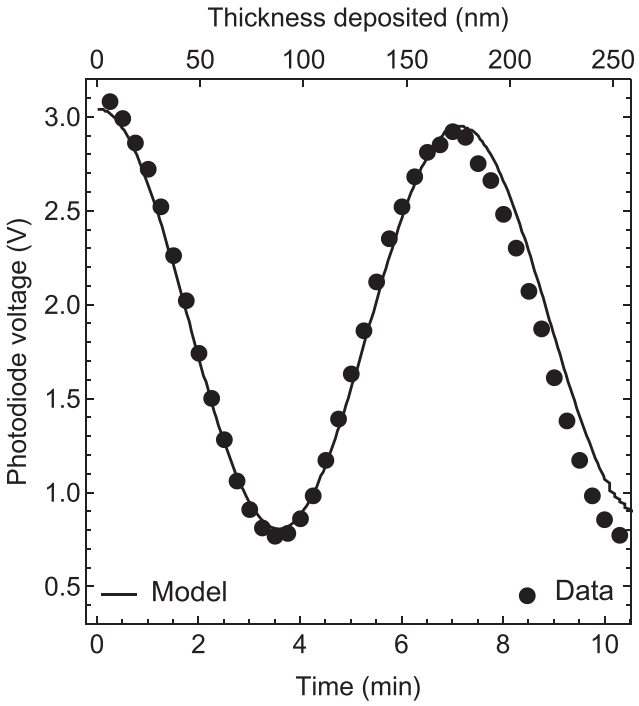

Figure 1. Laser interferometer photodiode voltage (points) for experimental values and model fit (solid line) versus time during the formation of water ice at 10 K from Milli-Q water at a pressure of 1.6×10^{-7} mbar.

Water ice films with thicknesses of up to 258 nm were deposited at a base pressure of 1×10^{-7} mbar from a nozzle via a needle valve connected to a glass bottle containing Milli-Q water. The water was purged of dissolved gases in several cycles of freezing and heating. The film thickness was monitored with the laser interferometric method described in Muntean et al. (2015); briefly, a photodiode detector monitored the intensity of $\lambda = 405$ nm laser light reflected from the ice film and KBr substrate. The angle of incidence of the light on the substrate was 45°.

Fig. 1 shows the laser interferometer photodiode detector voltage as a function of time (filled circles) during the water ice deposition process. The solid line is a model fit to the experimental data based on laws of reflection and refraction (see Muntean et al. 2015 for details). This enabled the refractive ice of the water ice to be determined and hence the ice density to be calculated. We obtained a best-fitting value of $n = 1.28 \pm 0.05$. Using the Lorentz–Lorenz equation from Fulvio et al. (2009), we calculated an ice density of $\rho = 0.79 \pm 0.02$ g cm^{-3}. These results are in good agreement with values of $n = 1.29 \pm 0.01$ and $\rho = 0.82$ g cm^{-3} measured by Westley, Baratta & Baragiola (1998) by reflection of $\lambda = 435.8$ nm light from a water ice film deposited at $T = 20$ K. We also note that Wood & Roux (1982) measured the refractive index of water ice deposited at 20 K, 50 K and 80 K for 632.8 nm light and found a constant value of 1.32 for all three temperatures.

3 RESULTS

The water ice was irradiated at $T = 10$ K and 45° incidence with singly charged C^+, N^+, O^+ and Ar^+ ions and doubly charged C^{2+}, N^{2+} and O^{2+} ions. Fig. 2 shows the photodiode detector voltage as a function of ion dose for irradiation of an initially 258 nm thick water ice film, at 10 K by 4 keV O^+ ions. The solid line shown in Fig. 2 is a model fit using the refractive index and density determined above.

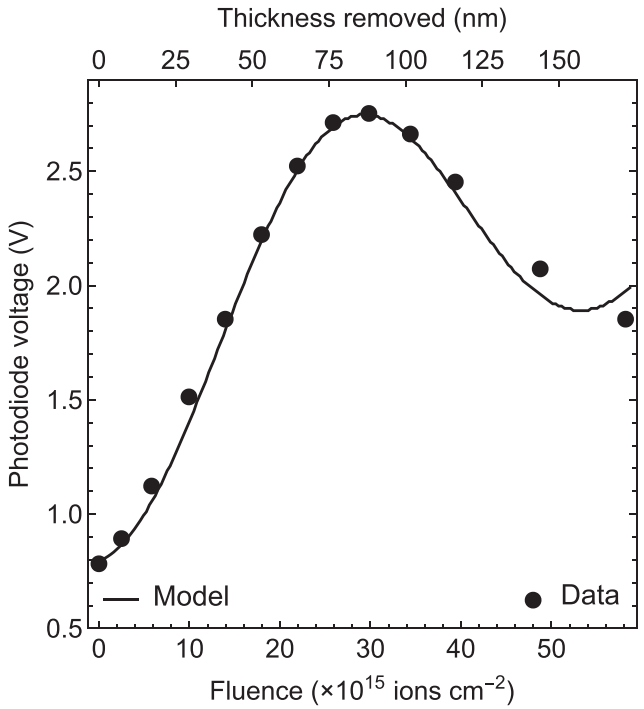

Figure 2. Laser interferometric data (points) and sputtering model (solid line) for 4 keV O^+ on a 258.4 nm water ice film irradiated at 10 K.

The fitted curve starts to increase before the second minimum is reached. This might be due to the irradiated ice films beginning to scatter the laser light and resulting in a loss of coherence. However, this does not affect our results as we have a good measurement of the first maximum, which is what is required for an accurate measurement of the ice thickness. The upper horizontal scale in Fig. 2 indicates the thickness of ice removed determined by the model, which was used to calculate the sputtering yield of $n(H_2O)$/ion, *viz.* the number of water molecules removed per incident ion.

Figs 3 and 4 show the number of water molecules removed as a function of fluence for 4 keV singly charged C^+, N^+ and O^+ and for 4 keV doubly charged C^{2+}, N^{2+} and O^{2+} ions, respectively. The ion beam intensity varied both for individual ions and range of ions studied, thus we express it in fluence rather than flux. Typically ion fluxes averages were about 1.8×10^{12} ions cm^{-2} s^{-1} for doubly charged ions and 9×10^{12} ions cm^{-2} s^{-1} for singly charged ions. From the slopes of linear regressions fitted to the experimental data and the measured ice density and refractive index, the sputtering yields for each ion species were calculated and are shown in Table 1. Taking our uncertainty in the fitted refractive index and propagating it through this analysis gives a total error budget of up to 20 per cent. We note that the fitting error in Figs 3 and 4 is ∼0.1 per cent.

Our experimental sputter yields for singly charged ions have been compared with theoretical values predicted by the model developed by Famá et al. (2008), given by the equation below.

$$Y(E, m_1, Z_1, \theta, T) = \frac{1}{U_0}\left(\frac{3}{4\pi^2 C_0}\alpha S_n + \eta S_e^2\right) \times \left(1 + \frac{Y_1}{Y_0}\exp\frac{-E_0}{kT}\right)\cos^{-f}\theta. \quad (1)$$

Famá's model predicts the sputtering yield as a result of ion irradiation of water ice at temperatures T from 10 K to 140 K, with ion energies E up to 100 keV and projectile ions with mass m_1, atomic

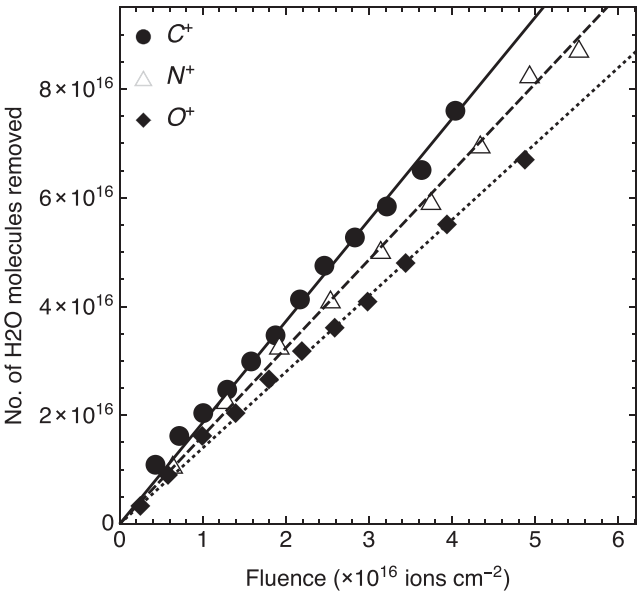

Figure 3. Number of H_2O molecules removed by 4 keV singly charged ions on water ice at 10 K as a function of ion dose.

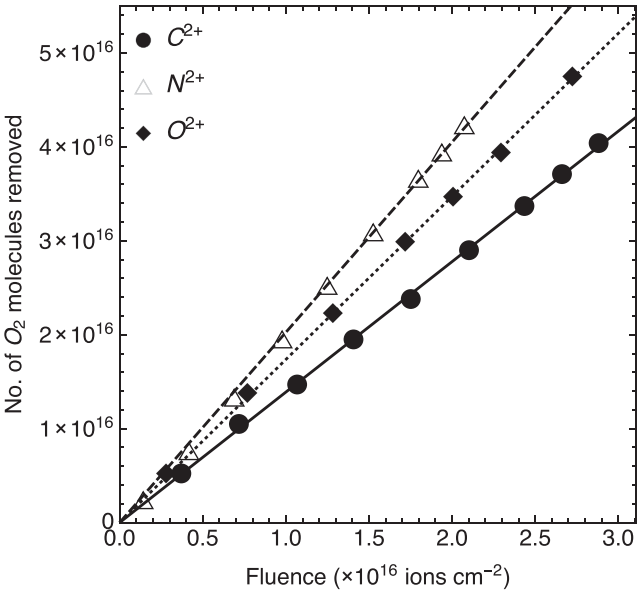

Figure 4. Number of O_2 molecules removed by 4 keV singly charged ions on water ice at 10 K as a function of ion dose.

Table 1. Experimental and theoretical values for sputtering yield of water ice (molecules per incident ion) at 10 K by 4 keV singly and doubly charged ions. The uncertainties shown are the total experimental errors.

	n	ρ (g cm^{-3})	$Y(H_2O)$ expt.	$Y(H_2O)$ theory
C^+	1.282	0.799	10.5 ± 2.1	7.3
N^+	”	”	9.2 ± 1.8	8.8
O^+	”	”	7.9 ± 1.6	9.7
Ar^+	”	”	19.8 ± 4.0	17.1
C^{2+}	”	”	7.8 ± 1.6	–
N^{2+}	”	”	11.4 ± 2.3	–
O^{2+}	”	”	9.8 ± 1.8	–

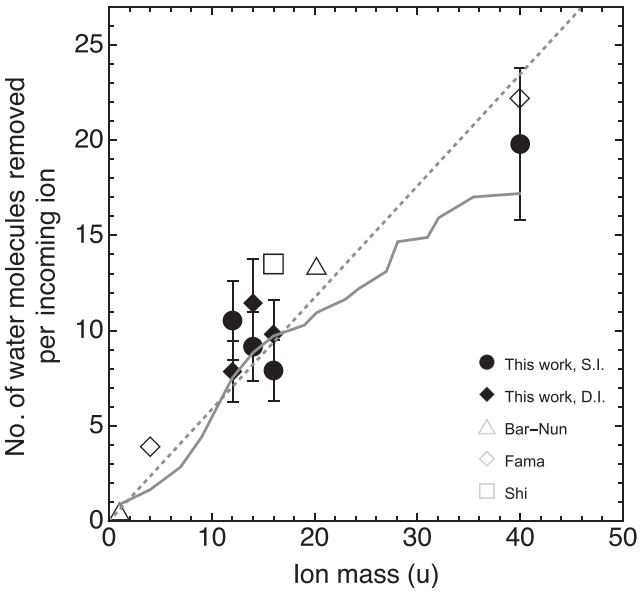

Figure 5. Sputtering yield per incoming ion as a function of ion mass. Our experimental results are marked as circles (filled symbols indicate singly ionized species and open symbols correspond to doubly ionized species.) Other symbols indicate experimental data by other authors (Bar-Nun et al. 1985; Shi et al. 1995; Famá et al. 2008). The solid line indicates the theoretical yield as a function of projectile mass, and the dashed line shows a simple linear fit (slope 0.59 ± 0.03) to all experimental data.

number Z_1 and incident angle θ. Our sputtering experiments were carried at a constant temperature (10 K) and an ion energy of 4 keV which means $\frac{Y_1}{Y_0} \exp \frac{-E_0}{kT} \simeq 0$. Also, the incidence angle, θ, was 45° for all the experiments. S_n and S_e are the nuclear and electronic stopping cross-sections, respectively, which were calculated using the standard Stopping Range of Ions in Matter (SRIM[1]) software. f denotes the power of the angular scattering function, α is a function of the mass ratio between the target and the projectile atomic masses and η is a function of the atomic number of the projectile. The empirical formulae used for obtaining the energy-independent values of η, α and f are explained in detail in Famá et al. (2008). $U_0 = 0.45$ eV is the binding energy, and $C_0 = 1.81$ Å^2 is a constant which is related to the differential cross-section for elastic scattering in the binary collision approximation (Sigmund 1981).

Table 1 summarizes the experimental and the predicted values for the sputtering yield of water ice when bombarded with singly and doubly charged ions. It can be clearly seen that the sputtering yield for both singly and doubly charged ions are the same within the experimental error. In Fig. 5, we plot our experimental values for the sputtering yield together with previous measurements in the literature. Our experimentally determined values for the sputtering yields are consistent with previous reports. For example, Famá et al. (2008) measured a sputtering yield for Ar^+ at normal incidence of 12 molecules per incident ion. This equates to 21.8 molecules per ion at 45° incidence, consistent with our measured value of 19.8 ± 4.0 molecules per ion. Recently, Galli et al. (2015) have measured the sputtering yield of porous NaCl water ice at 90 K for a range of ions with energies between 1 and 30 keV; the values obtained are consistent with all the data shown in Fig. 5. The data of Galli et al. are not plotted however, as the uncertainties of their measurements extend beyond the range of the ordinate. In Fig. 5, we also show the

[1] http://www.srim.org/

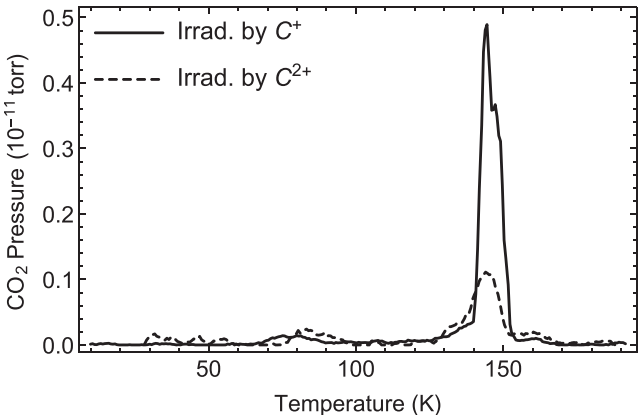

Figure 6. TPD profile for CO_2 produced through irradiation of H_2O ice by C^+ and C^{2+} (total dose 10^{16} ions in each case). The dominant TPD peak occurs at $T = 144.4 \pm 0.1$ K, while two lower peaks are found at $T = 84.7 \pm 0.4$ K and $T = 160.0 \pm 0.3$ K.

Table 2. Temperature-programmed desorption temperature peaks seen in Figs 6 and 7. Peak properties (central temperature, T, and area under the curve, I, in units of K Torr) derived from Gaussian fits to the data.

	CO		CO_2	
Ion	T (K)	$I/10^{-11}$	T (K)	$I/10^{-11}$
C^+	42.5 ± 0.1	102.0 ± 3.5	78.0 ± 0.2	0.25 ± 0.02
C^+	145.5 ± 0.1	3.30 ± 0.39	145.5 ± 0.1	3.68 ± 0.29
C^+	160.0 ± 0.5	3.72 ± 0.86	160.0 ± 0.2	0.08 ± 0.01
C^{2+}	50.3 ± 0.3	239.3 ± 12.9	84.7 ± 0.4	0.35 ± 0.04
C^{2+}	145.1 ± 0.2	8.32 ± 1.02	144.4 ± 0.1	1.37 ± 0.08
C^{2+}	160.0 ± 0.1	4.76 ± 0.31	160.0 ± 0.3	0.22 ± 0.04

predicted values from the Famá et al. (2008) theoretical model and find good agreement. We note that there is a slight tendency for the model to underestimate the experimental yields, the reason for this is unclear.

In addition, TPD measurements were carried out after the irradiation by $^{13}C^+$ and $^{13}C^{2+}$ with a constant ramp rate of 1 K min^{-1}. As can be seen from Fig. 6 and Table 2, irradiation by C^+ produced more CO_2 than irradiation by C^{2+}, with a yield ratio of 2.1 ± 0.2. This situation was reversed in the case of CO as shown in Fig. 7, where the ratio of yields from C^+ and C^{2+} was 0.4 ± 0.02. For C^+ irradiation, the production ratio of CO/$CO_2 \simeq 27$. For C^{2+} irradiation, the production ratio of CO/$CO_2 \simeq 130$.

4 DISCUSSION

4.1 Outer Solar system sputtering rates

Our measured sputter yield can be used to estimate at what rate H_2O ice is removed from the surface of an outer Solar system object due to irradiation by ions in the SW. Taking an SW ion density of $n_i = 4.5$ cm^{-3} and velocity $v_i = 400$ km s^{-1} at 1 au (Johnson et al. 1983), we calculate a total ion flux at a nominal distance of $a = 42$ au of $v_i\, n_i\, a^{-2} = 10^5$ ions cm^{-2} s^{-1}. Table 3 lists the relative abundances used here, calculated using the Genesis measurement of He/H fluence in the SW (Reisenfeld et al. 2007) and the values for C/He, N/He and O/He from the Ulysses mission (von Steiger et al. 2000). We combine these measurements to give the predicted fluxes at 42 au for ions of H, He, C, N and O. Our O^+ irradiation

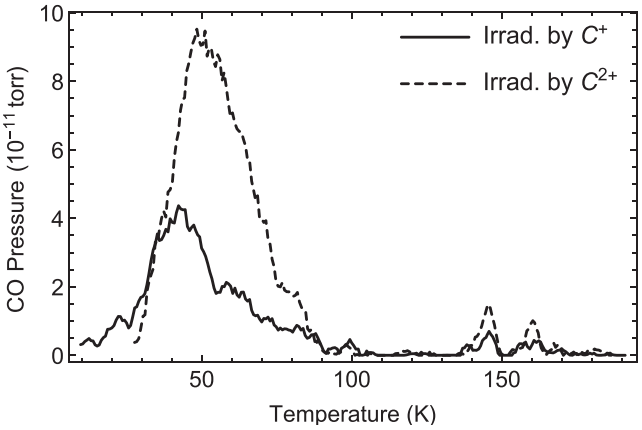

Figure 7. TPD profile for CO produced through irradiation of H_2O ice by C^+ and C^{2+} (total dose 10^{16} ions in each case). The dominant TPD peak occurs at $T = 42.5$ K after irradiation with C^+ and at $T = 50.3$ K after irradiation with C^{2+}, while two lower peaks are found near $T = 145$ K and $T = 160.0$ K in both cases.

Table 3. Solar wind properties and derived H_2O sputtering rate.

SW ion	Relative abundance	Flux at 42 au (cm^{-2} Myr^{-1})	Sputtering rate (nm Myr^{-1})
H	9.54×10^{-1}	3.1×10^{18}	3.20×10^{3}
He	4.58×10^{-2}	1.5×10^{17}	614
C	3.39×10^{-4}	1.1×10^{15}	13.6
N	3.98×10^{-5}	1.3×10^{14}	1.87
O	5.04×10^{-4}	1.6×10^{15}	27.0
Fe	5.54×10^{-5}	1.8×10^{14}	10.4

experiment indicates that sputtering erodes 86 nm of H_2O ice for a fluence of 4.5×10^{15} O^+ ions (Fig. 2). As seen in Fig. 5, this sputter yield scales as $0.59\, m_i$ where m_i is the mass of the ion in amu. Using these figures, we calculate in Table 3 the expected erosion rate for H_2O at 42 au due to sputtering by SW ions.

We find that proton erosion dominates, agreeing with expectations. It is also clear that sputtering will significantly erode and alter the optically active surface layers of ice in the trans-Neptunian region on extremely short time-scales relative to dynamical lifetimes of observed objects of $\geq 4.5 \times 10^9$ yr (Duncan, Levison & Budd 1995; Morbidelli, Levison & Gomes 2008). Other laboratory experiments have investigated the reddening of ices due to ion irradiation. According to the measurements of Strazzulla et al. (2003a) and Brunetto & Roush (2008), it optimistically takes $\sim 10^9$ yr to produce a 1 micron-deep reddened irradiation mantle. Sputtering by SW ions to a comparable depth is three orders of magnitude faster. This leads us to two possibilities: Either sputtering does not remove the red irradiation mantle hypothesized to exist on outer Solar system icy bodies, or the material is naturally red and reddening by ion irradiation is not a dominant effect.

We point out, however, that UV irradiation is an alternative pathway to the production of complex molecules (Bernstein, Allamandola & Sandford 1997), a process that may occur on significantly faster time-scales than the ion-induced changes. Also, an initial composition of complex hydrocarbons can give rise to significant reddening on dramatically shorter time-scales (Kaňuchová et al. 2012). As such, we suggest an appropriate amount of caution when interpreting reddening time-scales implied by laboratory measurements.

Sputtering of surface ices may be even more important for water-ice-rich Centaur objects evolving inwards from the trans-Neptunian region into the giant planet region. Many Centaurs have spectroscopically confirmed that H_2O ice absorption bands on their surfaces (Barkume, Brown & Schaller 2008; Barucci et al. 2011). Lifetimes of Centaurs typically lie in the range 10–90 Myr (Tiscareno & Malhotra 2003; Volk & Malhotra 2013). At ~10 au, the erosion rate will be $(42/10)^2 \sim 20$ times faster, so the SW will erode $\simeq$0.1–1 mm of H_2O ice on the surface of a Centaur during its dynamical lifetime. CO and CO_2 ices could also be present and will sublimate at these distances, although the observed activity in a small number of Centaurs may be due to this or due to crystallization of amorphous H_2O ice (Jewitt 2009; Guilbert-Lepoutre 2012). Our results show that even without sublimation or crystallization, pure H_2O ice will not survive unchanged. Therefore, we conclude that the optically active surfaces of all ice-rich bodies beyond Jupiter will be significantly modified.

4.2 Formation of CO and CO_2 by carbon ions

Our TPD results can be interpreted qualitatively in terms of CO and CO_2 forming in the H_2O ice as a result of irradiation by C^+ and C^{2+}. It is interesting to compare these results with TPD measurements of Collings et al. (2004), who investigated separate water ices with CO and with CO_2 on the surface and with CO and with CO_2 in the bulk. Surface samples were prepared by deposition on top of water ice and samples with bulk CO and CO_2 were prepared by co-deposition of either CO or CO_2 with H_2O. In our experiments, the majority of CO_2 desorption occurs at $T \sim 145$ K, 92 per cent $\pm$ 10 per cent in the case of C^+ irradiation and 71 per cent $\pm$ 5 per cent in the case of C^{2+} irradiation. This 145 K release was observed by Collings et al. (2004), who attribute this in their experiments to the volcano desorption of trapped CO_2 co-deposited with H_2O.

The release of CO_2 at around $T \sim 160$ K for both singly and doubly charged ion irradiation corresponds to co-desorption of trapped molecules with H_2O. However significantly less CO_2 was released at this temperature, 2 ± 0.3 per cent per cent for singly charged ions and 11 per cent $\pm$ 2 per cent for doubly charged ions. This differs from the results presented by Collings et al. (2004), who found roughly equal amounts desorbed at $T \sim 145$ K and $T \sim 160$ K when the CO_2 was co-deposited with H_2O.

For CO, our TPD results show major broad peaks at lower temperatures. In C^+ irradiation 93 per cent $\pm$ 4 per cent of the CO desorbs at $T = 42$ K, whereas in C^{2+} irradiation 92 per cent $\pm$ 2 per cent desorbs at $T = 50$ K. The peaks at $T = 145$ K and $T = 160$ K that correspond to volcano desorption and co-desorption, respectively, are minor features. Similar desorption features were observed by Collings et al. (2004) for CO both deposited on to a pre-adsorbed H_2O film, and co-deposited with H_2O. They also observed broad desorption peaks at low temperatures, but with similar amounts of CO released at the higher temperatures. The dominance of the low temperature peaks in the CO production, particularly in the case of C^{2+}, suggests that charge-dependent dissociation processes are occurring at or close to the surface of the water ice. In the case of CO_2, the majority is trapped below the surface layers within the H_2O matrix. It is interesting to note that different chemical reactions due to irradiation have been observed in layered $H_2O/CO/H_2O$ films in which CO layers were buried under amorphous solid water films of different thicknesses and then irradiated with 100 eV electrons Petrik et al. (2014). They found that the products formed from the oxidation and reduction/hydrogenation of CO were different for buried depths of up to 50 monolayers compared to products

of CO at depths of more than 50 monolayers. Our work suggests a depth-dependent effect in CO and CO_2 production.

Our yields in Table 2 imply that the mechanism for the formation of CO_2 is more efficiently driven by C^+ irradiation by approximately a factor of 2 compared to C^{2+} irradiation. A similar result was found by Dawes et al. (2007), who irradiated water ice at 30 K and 90 K with 4 keV C^+ and C^{2+} and measured CO_2 formation as a function of ion dose. They conclude that the CO_2 yield for singly charged ions is greater than for doubly charged ions, in qualitative agreement with our findings.

A significant finding from our TPD measurements was the observed large production rate of CO relative to CO_2. 4 keV C ions have a maximum penetration depth in water ice of 500 Å with a peak range of 236 Å. If in our case, we take the peak range and the thickness removed (1700 Å), this means only 14 per cent of the C^{2+} ions that can remain implanted to form CO and CO_2. Therefore, for a total fluence for C^{2+} of 2.9×10^{16} ions cm^{-2}, the maximum amount of retained ions becomes 2.1×10^{15} ions cm^{-2}. For a production yield of $\sim$0.5, a beam area of $1.77 \times 10^{-1} cm^2$ and a measured abundance of $CO/CO_2 = 130$, we have calculated an upper limit of the CO_2 produced to be 1.4×10^{12} molecules. In their previous study of 4 keV C-ion bombardment of H_2O ice, Dawes et al. (2007) did not observe any CO. However, we note that their lowest experimental temperature was 30 K. This is where the sublimation of CO starts according to both our TPD measurements (Fig. 7) and those of Collings et al. (2004). Therefore, we propose that as the CO formed preferentially at the surface, it was immediately sublimated during the Dawes et al. (2007) study, thereby accounting for the lack of subsequent spectral Fourier Transform Infrared Spectroscopy signatures.

Finally, it is interesting to note that in a 30 keV study at 10 K by Lv et al. (2012) and Strazzulla et al. (2003b) CO was not observed. This intriguing result may imply that CO formation by carbon ion bombardment of low-temperature ice is highly energy dependent, and deserves further study.

5 CONCLUSIONS

We have measured the sputtering yield from irradiated ice at 10 K by 4 keV singly charged (C^+, N^+, O^+ and Ar^+) and doubly charged ions (C^{2+}, N^{2+} and O^{2+}). In the case of singly charged ions, the sputtering yields have been compared with a theoretical model from Famá et al. (2008) and overall our measurements are in line with previous results and the model's predictions. Within experimental uncertainties, the sputtering yield of water ice does not depend on whether the projectiles are singly or doubly charged ions. We confirm that SW sputtering of fresh ice surfaces in the Kuiper belt and Centaur region can erode H_2O on dynamically relevant timescales.

TDP showed that CO formation dominates over CO_2 formation. However, $^{13}C^{2+}$ is relatively more efficient in forming ^{13}CO while $^{13}C^+$ is relatively more efficient in forming $^{13}CO_2$. The majority of the ^{13}CO desorbs at $T \simeq 42$ K which suggests that this species is produced close to the surface of the water ice, whereas the majority of the $^{13}CO_2$ desorbs at $T \simeq 145$ K and indicates that CO_2 is formed below the surface.

ACKNOWLEDGEMENTS

We thank M. Famá for useful comments and suggestions. We thank the Leverhulme Trust for support through a Research Project Grant RPG-2013-389. PL is grateful for support from the Royal Society in the form of a Newton Fellowship. Part of this work was supported by the European Commission's 7th Framework Programme under Grant Agreement No. 238258.

REFERENCES

Bagenal F., Cravens T. E., Luhmann J. G., McNutt R. L. Jr Cheng A. F., 1997, in Stern S. A., Tholen D. J., eds, Pluto and Charon. Oxford Univ. Press, Oxford, p. 523
Bar-Nun A., Herman G., Rappaport M., Mekler Y., 1985, Surf. Sci., 150, 143
Baragiola R., Vidal R., Svendsen W., Schou J., Shi M., Bahr D., Atteberrry C., 2003, Nucl. Instrum. Methods Phys. Res. B, 209, 294
Barkume K. M., Brown M. E., Schaller E. L., 2008, AJ, 135, 55
Barucci M. A., Alvarez-Candal A., Merlin F., Belskaya I. N., de Bergh C., Perna D., DeMeo F., Fornasier S., 2011, Icarus, 214, 297
Bernstein M. P., Allamandola L. J., Sandford S. A., 1997, Adv. Space Res., 19, 991
Brown M. E., Hill R. E., 1996, Nature, 380, 229
Brown W., Lanzerotti L., Poate J., Augustyniak W., 1978, Phys. Rev. Lett., 40, 1027
Brown W., Augustyniak W., Lanzerotti L., Johnson R., Evatt R., 1980, Phys. Rev. Lett., 45, 1632
Brown M. E., Schaller E. L., Fraser W. C., 2012, AJ, 143, 146
Brunetto R., Roush T. L., 2008, A&A, 481, 879
Brunetto R., Barucci M. A., Dotto E., Strazzulla G., 2006, ApJ, 644, 646
Christiansen J., Carpini D. D., Tsong I., 1986, Nucl. Instrum. Methods Phys. Res. B, 15, 218
Collings M. P., Anderson M. A., Chen R., Dever J. W., Viti S., Williams D. A., McCoustra M. R. S., 2004, MNRAS, 354, 1133
Cooper B., Tombrello T., 1984, Radiat. Eff., 80, 203
Dalton J. B., Cruikshank D. P., Stephan K., McCord T. B., Coustenis A., Carlson R. W., Coradini A., 2010, Space Sci. Rev., 153, 113
Dawes A., Hunniford A., Holtom P. D., Mukerji R. J., McCullough R. W., Mason N. J., 2007, Phys. Chem. Chem. Phys., 9, 2886
Duncan M. J., Levison H. F., Budd S. M., 1995, AJ, 110, 3073
Famá M., Shi J., Baragiola R. A., 2008, Surf. Sci., 602, 156
Florinski V., Jokipii J. R., Alouani-Bibi F., le Roux J. A., 2013, ApJ, 776, L37
Fulvio D., Sivaraman B., Baratta G., Palumbo M., Mason N., 2009, Spectrochim. Acta Part A, 72, 1007
Galli A. et al., 2015, preprint (arXiv:1509.04008)
Guilbert A., Alvarez-Candal A., Merlin F., Barucci M. A., Dumas C., de Bergh C., Delsanti A., 2009, Icarus, 201, 272
Guilbert-Lepoutre A., 2012, AJ, 144, 97
Hall D. T., Strobel D. F., Feldman P. D., McGrath M. A., Weaver H. A., 1995, Nature, 373, 677
Hudson R. L., Moore M. H., 2001, J. Geophys. Res., 106, 33275
Jewitt D., 2009, AJ, 137, 4296
Johnson R. E., 1990, Energetic Charged-Particle Interactions with Atmospheres and Surfaces. Springer-Verlag, Berlin
Johnson R. E., Lanzerotti L. J., Brown W. L., Augustyniak W. M., Mussil C., 1983, A&A, 123, 343
Johnson R. E., Famá M., Liu M., Baragiola R. A., Sittler E. C., Smith H. T., 2008, Planet. Space Sci., 56, 1238
Kaňuchová Z., Brunetto R., Melita M., Strazzulla G., 2012, Icarus, 221, 12
Lunine J. I., 2006, in Lauretta D. S., McSween H. Y. Jr., eds, Origin of Water Ice in the Solar System, Meteorites and the Early Solar System II. Univ. Arizona Press, Tucson, p. 309
Lv X. Y. et al., 2012, A&A, 546, A81
Morbidelli A., Levison H. F., Gomes R., 2008, The Dynamical Structure of the Kuiper Belt and Its Primordial Origin. Univ. Arizona Press, Tucson, p. 275
Muntean E. A., Lacerda P., Field T. A., Fitzsimmons A., Hunniford C. A., McCullough R. W., 2015, Surf. Sci., 641, 204
Petrik N. G., Monckton R. J., Koehler S. P. K., Kimmel G. A., 2014, J. Chem. Phys., 140, 204710

Reisenfeld D. B. et al., 2007, Space Sci. Rev., 130, 79
Schenk P., Hamilton D. P., Johnson R. E., McKinnon W. B., Paranicas C., Schmidt J., Showalter M. R., 2011, Icarus, 211, 740
Shi M., Baragiola R. A., Grosjean D. E., Johnson R. E., Jurac S., Schou J., 1995, J. Geophys. Res., 100, 26387
Sigmund P., 1981, Sputtering by Ion Bombardment Theoretical Concepts. Springer-Verlag, Berlin p. 9
Strazzulla G., Cooper J. F., Christian E. R., Johnson R. E., 2003a, C. R. Phys., 4, 791
Strazzulla G., Leto G., Gomis O., Satorre M. A., 2003b, Icarus, 164, 163
Teolis B. D., Vidal R. A., Shi J., Baragiola R. A., 2005, Phys. Rev. B, 72, 245422
Teolis B., Shi J., Baragiola R., 2009, J. Chem. Phys., 130, 134704
Tiscareno M. S., Malhotra R., 2003, AJ, 126, 3122
Vidal R., Teolis B., Baragiola R., 2005, Surf. Sci., 588, 1
Volk K., Malhotra R., 2013, Icarus, 224, 66
von Steiger R. et al., 2000, J. Geophys. Res., 105, 27217
Westley M., Baratta G., Baragiola R., 1998, J. Chem. Phys., 108, 3321
Wood B., Roux J., 1982, J. Opt. Soc. Am., 72, 720

This paper has been typeset from a TEX/LATEX file prepared by the author.